The Torsional Buckling and Writhing of a Simply-Supported Rod Hanging under Gravity

D.M. Stump [1]
Department of Mathematics
The University of Queensland
St. Lucia QLD 4072
Australia

A.R. Champneys [2]
Department of Engineering Mathematics
University of Bristol
Bristol BS8 1TR
United Kingdom

and

G.H.M. van der Heijden [3]
Centre for Nonlinear Dynamics
University College London
London WC1E 6BT
United Kingdom

February 17, 1999

[1]email dms@maths.uq.oz.au
[2]email a.r.champneys@bristol.ac.uk
[3]email g.heijden@ucl.ac.uk

Abstract

The problem of a finite-length simply-supported rod hanging under gravity and subject to a prescribed tangential twist Tw is studied using asymptotic and numerical methods. A three-dimensional formulation of the problem is given in which a small parameter ε^2 measures the relative sizes of bending and gravitational forces. For small values of Tw, the rod shape is found by singular perturbation methods and consists of an *outer* catenary-like solution and an *inner* boundary layer solution. Large twist $Tw = O(1/\varepsilon)$ of an almost straight rod produces a torque on the order of the Greenhill buckling level and is shown numerically to cause buckling into a modulated helix-like spiral with period of $O(\epsilon)$ superimposed onto a parabolic sag across the spanned distance. Multiple scale methods are used in this parameter regime to obtain an approximate description of the post-buckled solution. This analysis is found to capture all the broad features indicated by the numerics. As Tw is further increased, the deformation may localise and the rod jump into a self-intersecting writhed shape.

1 Introduction

The study of the buckling of long, thin, straight rods under applied axial tension and moment goes at least as far back as Kirchhoff (1859). Such problems arise in many applications across engineering and physical science, ranging from the failure of undersea cables and pipelines — e.g. Coyne (1990) — to the helical spiral inversion seen in the tendrils of climbing plants (Goriely & Tabor 1998). Greenhill (1883) showed that under only remote tension T and moment Q a rod of length L first buckles into a helical shape when

$$\frac{4\pi^2 B^2}{L^2} = Q^2 - 4BT, \tag{1}$$

where B is the bending rigidity of the rod. The helical solution was further analysed in the treatise by Love (1927). Also see Timoshenko & Gere (1961) for a more modern engineering treatment, and the book by Antman (1995) for a mathematical account of the general theory of rod mechanics.

It is well known that in the absence of torsion, a rod hanging under gravity while being pulled horizontally will hang in a catenary. If torsion is applied, phenomenological experiments — e.g. Thompson & Champneys (1996) — indicate that if the tension is sufficiently high the effect of gravity appears not to destroy the initial buckling into a helix. Indeed in Champneys, van der Heijden & Thompson (1997) gravity was written as one of several perturbations to the 'perfect' problem, but, unlike non-symmetric cross-section, intrinsic curvature and shear deformation, the effect of gravity was not analysed. The form of the perturbation caused by gravity was much harder because with the others the force and moment equilibrium equations when written in a material co-ordinate basis could be analysed as an autonomous dynamical system which is decoupled from the *Frenet-Seret* equations for the centreline of the rod. Because this is not possible in the case of gravity, one cannot use the trick of passing to an infinitely long rod and employing the (Kirchhoff) analogy with an initial-value problem (see Kehrbaum & Maddocks (1997) for the details of this analogy).

A recent treatment by Stump & van der Heijden (1998) provides the starting point for the present analysis. Motivated by the problem of an underwater pipeline being laid from a barge, they study a finite-length rod, clamped at both ends, subject to tension and a moderate amount of twist supplied by rotations of the barge. A nondimensionalisation introduces a small parameter ε which is the square root of

the ratio of characteristic bending and gravitational forces. Since the total twist Tw inserted into the rod is $O(1)$, the solution is represented as a matched asymptotic expansion with an *outer* catenary-like layer and *inner* bending boundary layers on the $O(\varepsilon)$ length-scale.

The present paper considers a (symmetric, unshearable) rod subject to simply-supported boundary conditions. The general problem is formulated for arbitrary span length d and arbitrary levels of inserted twist Tw. For Tw of $O(1)$, the boundary-layer analysis of Stump & van der Heijden (1998) is adapted for the present boundary conditions, giving a catenary-like solution in the centre of the span with boundary layers at the ends. The truncated analytical results agree well with numerical computations. This solution breaks down at $Tw = O(1/\varepsilon)$.

Accurate numerics are used to explore the effects of large Tw values. For small ϵ, the solution remains essentially a catenary until a value of Tw consistent with the Greenhill buckling torque is reached. At this point the solution changes markedly and is given approximately by a catenary and a superimposed helix with a period of $O(\varepsilon)$. As Tw is increased further the helix angle tightens and the centre of the span rises. Eventually, after all the slack is taken up, the helical deformations begin to localize. Motivated by these numerical results, a heuristic multiple-scale analysis in the outer region is used to separate the two leading components of the solution. The results explain all the broad features of the post-buckling path.

The paper is ordered as follows. Section 2 develops the mathematical model for the rod. Section 3 considers the low-twist case where $Tw = O(1)$. Results obtained by asymptotic methods are compared with numerical work. Section 4 deals with the high-twist case for small ϵ. Detailed numerical results are presented first which suggest the scalings for the multiple-scale analysis which then follows. Section 5 closes the study with some remarks.

2 The Model

A long, thin, inextensible, unshearable rod of natural length L and with circular cross-section is assumed to span the x-axis over the region $(0 \leq x \leq d)$ of a Cartesian co-ordinate system, as shown in Fig. 1. The arclength co-ordinate s $(0 \leq s \leq L)$ runs along the rod, and gravity points in the negative $\boldsymbol{j}$-direction. The configuration of the rod's centreline is specified by the position vector $\boldsymbol{R}(s)$, and the rod is assumed to have a total twist Tw. For simplicity, the rod is taken as linear elastic.

Since the cross-section is circular, the equilibrium equations for such a rod can be formulated entirely in terms of the Frenet derivatives of its centreline without the need for the more general Cosserat formulation. Thus, the equations for force and moment balance governing the equilibrium shape of the rod with centreline $\boldsymbol{R}(s)$ are written as

$$\begin{aligned} &(T\boldsymbol{R}')' + \boldsymbol{V}' - mg\,\boldsymbol{j} = \boldsymbol{0}, \\ &(Q\boldsymbol{R}')' + \boldsymbol{M}' + \boldsymbol{R}' \times \boldsymbol{V} = \boldsymbol{0} \end{aligned} \tag{2}$$

(Stump & van der Heijden 1998). Here: $T(s)$ is the tensile component of force; $\boldsymbol{V}(s)$ is the shear force; mg is the weight per unit-length of rod; $\boldsymbol{M}(s)$ is the bending moment; and Q is the twisting moment. These equations are augmented with the inextensibility condition; the normality of the shear force and the tangent vectors; and the linear constitutive law linking bending moment and curvature:

$$\begin{aligned} &\boldsymbol{R}' \cdot \boldsymbol{R}' = 1, \\ &\boldsymbol{R}' \cdot \boldsymbol{V} = 0, \\ &\boldsymbol{M} = B(\boldsymbol{R}' \times \boldsymbol{R}''). \end{aligned} \tag{3}$$

It is straightforward to show that the torque Q is constant along the rod by forming

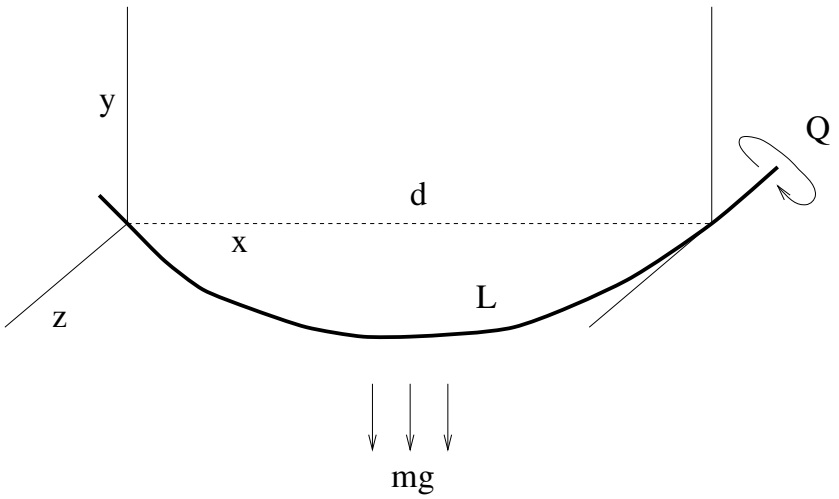

Figure 1: Sketch of the physical set-up.

the dot product of $\boldsymbol{R}'$ with $(2)_2$ to obtain $Q' = 0$. The rate of cross-sectional rotation N' and the twist Tw are linked to Q by the constitutive law

$$Q = KN' = \frac{2\pi KTw}{L}. \tag{4}$$

Here $B = EI$ and $K = GJ$ are the bending and torsional rigidities, respectively, and: E is Young's modulus; G is the shear modulus; $I = \pi a^4/4$ is the second moment of area (a being the radius of the rod); and $J = \pi a^4/2$ is the polar moment of inertia.

Equations (2)–(4) may be made dimensionless against the characteristic length L and force mgL by setting

$$\overline{s} = \frac{s}{L}, \quad \overline{\boldsymbol{M}} = \frac{\boldsymbol{M}}{mgL^2}, \quad \overline{Q} = \frac{Q}{mgL^2}, \quad \overline{T} = \frac{T}{mgL}, \quad \overline{\boldsymbol{V}} = \frac{\boldsymbol{V}}{mgL},$$

and by introducing the dimensionless parameters

$$\varepsilon^2 = \frac{B}{mgL^3} \quad \text{and} \quad \kappa = \frac{K}{B}. \tag{5}$$

The value of $\kappa = 1/(1+\nu)$ (ν is Poisson's ratio) is of $O(1)$, while the *stiffness* parameter ε is typically $<< O(1)$.

Henceforth we deal exclusively with dimensionless variables and therefore drop the overbars. The dimensionless equations then become

$$\begin{aligned}
&(T\boldsymbol{R}')' + \boldsymbol{V}' - \boldsymbol{j} = \boldsymbol{0}\,,\\
&(Q\boldsymbol{R}')' + \boldsymbol{M}' + \boldsymbol{R}' \times \boldsymbol{V} = \boldsymbol{0},\\
&\boldsymbol{R}' \cdot \boldsymbol{R}' = 1,\\
&\boldsymbol{R}' \cdot \boldsymbol{V} = 0,\\
&\boldsymbol{M} = \varepsilon^2(\boldsymbol{R}' \times \boldsymbol{R}''),\\
&Q = \varepsilon^2\kappa N' = \varepsilon^2(2\pi\kappa Tw).
\end{aligned} \tag{6}$$

This system is reduced to a single vector equation by first integrating $(6)_1$ once to obtain

$$T\boldsymbol{R}' + \boldsymbol{V} - s\boldsymbol{j} + \boldsymbol{C} = \boldsymbol{0}, \tag{7}$$

where $\boldsymbol{C}$ is as yet an unknown vector. Next, formation of the scalar product of (7) with $\boldsymbol{R}'$ along with the use of $(6)_4$ and the inextensibility condition $(6)_3$ leads to the expression for the tension:

$$T = s(\boldsymbol{R}' \cdot \boldsymbol{j}) - \boldsymbol{C} \cdot \boldsymbol{R}'. \tag{8}$$

Finally, the use of (7) and (8) to eliminate $\boldsymbol{V}$ and T from $(6)_2$ followed by the formation of the vector product with $\boldsymbol{R}'$ produces the single second-order equation

for $\boldsymbol{R}'$:

$$\varepsilon^2 \left[2\pi\kappa T w(\boldsymbol{R}' \times \boldsymbol{R}'') - \boldsymbol{R}''' - \boldsymbol{R}'(\boldsymbol{R}'' \cdot \boldsymbol{R}'')\right] + \left[s(\boldsymbol{R}' \cdot \boldsymbol{j}) - \boldsymbol{C} \cdot \boldsymbol{R}'\right] \boldsymbol{R}' - s\boldsymbol{j} + \boldsymbol{C} = \boldsymbol{0}. \tag{9}$$

This study is specifically interested in the dimensionless *simply-supported* boundary conditions

$$\begin{array}{ll} \boldsymbol{R}(0) = \boldsymbol{0}, & \boldsymbol{R}''(0) = \boldsymbol{0}, \\ \boldsymbol{R}(1) = d\,\boldsymbol{i}, & \boldsymbol{R}''(1) = \boldsymbol{0}, \end{array} \tag{10}$$

in which the bending curvature vanishes at the ends of the rod. Equation (9) describes the shape of the rod subject to the boundary conditions (10). Also, we restrict consideration to shapes that are symmetric with respect to the centre of the span, as shown in Fig. 1.

3 Low-twist Analysis

In this section equation (9) is analysed under the assumption that Q is $O(\epsilon^2)$, or Tw is $O(1)$. The analysis closely follows Stump & van der Heijden (1998) to which we refer for more details. Since the equation obtained by putting $\epsilon = 0$ in (9) is of lower order than (9) itself, the boundary conditions (10) can not in general be satisfied, and we expect $O(\epsilon)$ boundary layers near both ends of the rod. In the following we first analyse the solution away from the ends (the *outer* solution), and then, after introducing the scaled distance $\xi = s/\epsilon$, study the solution in the boundary layers (the *inner* solutions). Finally, the solutions are patched together by matching with an intermediate co-ordinate.

3.1 The Outer Solution

The quantities $\boldsymbol{R}(s)$ and $\boldsymbol{C}$ are expanded in regular perturbation series in the parameter ϵ:

$$\begin{aligned} \boldsymbol{R}(s) &= \boldsymbol{R}_0(s) + \epsilon \boldsymbol{R}_1(s) + \epsilon^2 \boldsymbol{R}_2(s) + \ldots , \\ \boldsymbol{C} &= \boldsymbol{C}_0 + \epsilon \boldsymbol{C}_1 + \epsilon^2 \boldsymbol{C}_2 + \ldots , \end{aligned} \tag{11}$$

which are substituted into (9) to obtain a succession of equations in powers of ϵ, the first two of which are

$$\begin{aligned} O(1): \quad & [s(\boldsymbol{R}_0' \cdot \boldsymbol{j}) - \boldsymbol{C}_0 \cdot \boldsymbol{R}_0'] \, \boldsymbol{R}_0' - s\boldsymbol{j} + \boldsymbol{C}_0 = \boldsymbol{0}, \\ O(\epsilon): \quad & s(\boldsymbol{R}_0' \cdot \boldsymbol{j})\boldsymbol{R}_1' + s(\boldsymbol{R}_1' \cdot \boldsymbol{j})\boldsymbol{R}_0' - (\boldsymbol{C}_1 \cdot \boldsymbol{R}_0')\boldsymbol{R}_0' \\ & -(\boldsymbol{C}_0 \cdot \boldsymbol{R}_1')\boldsymbol{R}_0' - (\boldsymbol{C}_0 \cdot \boldsymbol{R}_0')\boldsymbol{R}_1' + \boldsymbol{C}_1 = \boldsymbol{0} \, . \end{aligned} \tag{12}$$

The use of the inextensibility condition $(3)_1$ provides the additional constraints that $\boldsymbol{R}_0' \cdot \boldsymbol{R}_0' = 1$ and $\boldsymbol{R}_0' \cdot \boldsymbol{R}_1' = 0$.

The $O(1)$ solution of (12) is obtained by introducing $\boldsymbol{R}_0 = x_0\boldsymbol{i} + y_0\boldsymbol{j} + z_0\boldsymbol{k}$ and $\boldsymbol{C}_0 = c_x\boldsymbol{i} + c_y\boldsymbol{j} + c_z\boldsymbol{k}$ into $(12)_1$ and solving the resulting set of equations by elementary means to obtain

$$\begin{aligned} x_0 &= -|c_x| \sinh^{-1}\left\{\frac{c_y - s}{\sqrt{c_x^2 + c_z^2}}\right\} + |c_x| \sinh^{-1}\left\{\frac{c_y}{\sqrt{c_x^2 + c_z^2}}\right\} + X_0 \, , \\ y_0 &= -\alpha\sqrt{c_x^2 + (c_y - s)^2 + c_z^2} + \alpha\sqrt{c_x^2 + c_y^2 + c_z^2} + Y_0 \, , \\ z_0 &= \frac{c_z}{c_x} x_0 + Z_0 \, , \end{aligned} \tag{13}$$

where $\alpha = c_x/|c_x|$, and (X_0, Y_0, Z_0) are additional constants of integration. This is the three-dimensional catenary lying in a plane making an angle $\chi = \arctan(c_z/c_x)$ with the $(\boldsymbol{i}, \boldsymbol{j})$ co-ordinate plane. The constants (c_x, c_y, c_z) are still unknown and will be determined in the matching process. We can already observe, however, that solutions come in pairs as the equations in (13) are invariant under a simultaneous sign change of c_x and c_z. (These correspond to the conventional downward hanging solution under tension, and the inverted arch-like solution under compression.)

The solution to the $O(\epsilon)$ equation is found from the formation of two successive vector products of $\boldsymbol{R}_0'$ with $(12)_2$, which yields:

$$\boldsymbol{R}_0' \times (\boldsymbol{R}_0' \times \boldsymbol{R}_1') \left[s(\boldsymbol{R}_0' \cdot \boldsymbol{j}) - \boldsymbol{C}_0 \cdot \boldsymbol{R}_0' \right] + \boldsymbol{R}_0' \times (\boldsymbol{R}_0' \times \boldsymbol{C}_1) = \boldsymbol{0}\,. \tag{14}$$

The use of the triple vector product and inextensibility gives

$$\boldsymbol{R}_1' = \frac{\boldsymbol{R}_0'(\boldsymbol{R}_0' \cdot \boldsymbol{C}_1) - \boldsymbol{C}_1}{s(\boldsymbol{R}_0' \cdot \boldsymbol{j}) - \boldsymbol{C}_0 \cdot \boldsymbol{R}_0'}. \tag{15}$$

The solution for $\boldsymbol{R}_1 = x_1\boldsymbol{i} + y_1\boldsymbol{j} + z_1\boldsymbol{k}$ and $\boldsymbol{C}_1 = d_x\boldsymbol{i} + d_y\boldsymbol{j} + d_z\boldsymbol{k}$ is obtained by using (13) along with elementary integrations to yield

$$\begin{aligned} \boldsymbol{R}_1(s) = \; & \{(-|c_x|c_z d_z + \alpha c_z^2 d_x) I_1(s) - |c_x| d_y \, I_2(s) + \alpha d_x \, I_3(s)\} \, \boldsymbol{i} \\ & + \{\alpha(c_x^2 d_y + c_z^2 d_y) I_1(s) - (\alpha c_z d_z + |c_x| d_x) I_2(s)\} \, \boldsymbol{j} \\ & + \{(-|c_x|c_z d_x + \alpha c_x^2 d_z) I_1(s) - \alpha c_z d_y \, I_2(s) + \alpha d_z \, I_3(s)\} \, \boldsymbol{k} \\ & + X_1\boldsymbol{i} + Y_1\boldsymbol{j} + Z_1\boldsymbol{k}, \end{aligned} \tag{16}$$

where (X_1, Y_1, Z_1) are integration constants and

$$\begin{aligned} I_1(s) &= -\frac{c_y - s}{(c_x^2 + c_z^2)\sqrt{c_x^2 + (c_y - s)^2 + c_z^2}}, \\ I_2(s) &= \frac{1}{\sqrt{c_x^2 + (c_y - s)^2 + c_z^2}}, \\ I_3(s) &= \frac{c_y - s}{\sqrt{c_x^2 + (c_y - s)^2 + c_z^2}} - \sinh^{-1}\left(\frac{c_y - s}{\sqrt{c_x^2 + c_z^2}}\right). \end{aligned}$$

3.2 The Inner Solution

Because we are interested in symmetric rod shapes, only the boundary layer near $s = 0$ needs to be considered. We introduce the scaled co-ordinate $\xi = s/\epsilon$ and write

$$\boldsymbol{R}(s) = \epsilon\hat{\boldsymbol{R}}(\xi) = \epsilon\hat{\boldsymbol{R}}_0(\xi) + \epsilon^2\hat{\boldsymbol{R}}_1(\xi) + \ldots. \tag{17}$$

so that the tangent has the form

$$\boldsymbol{R}'(s) = \hat{\boldsymbol{R}}'(\xi) = \hat{\boldsymbol{R}}_0'(\xi) + \epsilon\hat{\boldsymbol{R}}_1'(\xi) + \dots ,$$

where the prime denotes differentiation with respect to the appropriate argument.

In the boundary layer, (9) is written in terms of $\hat{\boldsymbol{R}}(\xi)$ by

$$\left[\epsilon\xi(\hat{\boldsymbol{R}}'\cdot\boldsymbol{j}) - \boldsymbol{C}\cdot\hat{\boldsymbol{R}}'\right]\hat{\boldsymbol{R}}' - \hat{\boldsymbol{R}}''' - \hat{\boldsymbol{R}}'(\hat{\boldsymbol{R}}''\cdot\hat{\boldsymbol{R}}'') + \epsilon 2\pi\kappa Tw(\hat{\boldsymbol{R}}'\times\hat{\boldsymbol{R}}'') - \epsilon\xi\boldsymbol{j} + \boldsymbol{C} = \boldsymbol{0}. \quad (18)$$

With $(11)_2$, (18) can be separated into a sequence of equations in ϵ, the first two of which are

$$\begin{aligned} O(1): \quad & (\boldsymbol{C}_0\cdot\hat{\boldsymbol{R}}_0')\hat{\boldsymbol{R}}_0' + \hat{\boldsymbol{R}}_0''' + \hat{\boldsymbol{R}}_0'(\hat{\boldsymbol{R}}_0''\cdot\hat{\boldsymbol{R}}_0'') = \boldsymbol{C}_0, \\ O(\epsilon): \quad & \xi(\hat{\boldsymbol{R}}_0'\cdot\boldsymbol{j})\hat{\boldsymbol{R}}_0' - (\boldsymbol{C}_1\cdot\hat{\boldsymbol{R}}_0')\hat{\boldsymbol{R}}_0' - (\boldsymbol{C}_0\cdot\hat{\boldsymbol{R}}_1')\hat{\boldsymbol{R}}_0' - \\ & (\boldsymbol{C}_0\cdot\hat{\boldsymbol{R}}_0')\hat{\boldsymbol{R}}_1' - \hat{\boldsymbol{R}}_1''' - \hat{\boldsymbol{R}}_1'(\hat{\boldsymbol{R}}_0''\cdot\hat{\boldsymbol{R}}_0'') - 2\hat{\boldsymbol{R}}_0'(\hat{\boldsymbol{R}}_1''\cdot\hat{\boldsymbol{R}}_0'') - \\ & \xi\boldsymbol{j} + 2\pi\kappa Tw(\hat{\boldsymbol{R}}_0'\times\hat{\boldsymbol{R}}_0'') + \boldsymbol{C}_1 = \boldsymbol{0}. \end{aligned} \quad (19)$$

The inextensibility condition is also expanded and leads to a series of equations: $\hat{\boldsymbol{R}}_0'\cdot\hat{\boldsymbol{R}}_0' = 1$; $\hat{\boldsymbol{R}}_0'\cdot\hat{\boldsymbol{R}}_1' = 0$; and so on. It is noted that for $O(1)$ values of Tw, twist appears first in the $O(\epsilon)$ equation. The boundary conditions (10) become

$$\begin{aligned} &\hat{\boldsymbol{R}}_0(0) = \hat{\boldsymbol{R}}_1(0) = \dots = \boldsymbol{0}, \\ &\hat{\boldsymbol{R}}_0''(0) = \hat{\boldsymbol{R}}_1''(0) = \dots = \boldsymbol{0}. \end{aligned} \quad (20)$$

The solution to the $O(1)$ equation is obtained by forming the vector product with $\hat{\boldsymbol{R}}_0'$ and integrating the result to get

$$\hat{\boldsymbol{R}}_0'\times\hat{\boldsymbol{R}}_0'' = \hat{\boldsymbol{R}}_0\times\boldsymbol{C}_0 + \boldsymbol{D}_0, \quad (21)$$

where $\boldsymbol{D}_0$ is a constant of integration. From (20) we have $\boldsymbol{D}_0 = \boldsymbol{0}$. Another cross product with $\hat{\boldsymbol{R}}_0'$ yields

$$\hat{\boldsymbol{R}}_0'' = -\hat{\boldsymbol{R}}_0'\times\left[\hat{\boldsymbol{R}}_0\times\boldsymbol{C}_0\right]. \quad (22)$$

This is the equation of the planar elastica. Since no bending moments are applied at the rod ends and twist is absent at the current level of approximation, the leading order rod shape $\hat{\boldsymbol{R}}_0$ is confined to a plane containing $\boldsymbol{i}$, the direction of the span vector connecting the ends of the rod, and $\boldsymbol{j}$, the line of gravity. It is convenient to define a set of basis vectors $(\boldsymbol{N}, \boldsymbol{k}, \boldsymbol{P})$ by

$$\boldsymbol{N} = \alpha\frac{\boldsymbol{C}_0}{|\boldsymbol{C}_0|}, \qquad \boldsymbol{P} = \boldsymbol{k}\times\boldsymbol{N}, \quad (23)$$

so that for the inner solution we can write

$$\hat{\boldsymbol{R}}_0(\xi) = \rho(\xi)\boldsymbol{P} + h(\xi)\boldsymbol{N}\,. \tag{24}$$

Inextensibility, the boundary conditions (20), and the requirement that $\boldsymbol{R}''$ vanish as $\xi \to \infty$ provide the limiting values

$$\rho(0) = h(0) = 0 \qquad \text{and} \qquad \lim_{\xi\to\infty} \rho(\xi)\rho'(\xi) = 0, \quad \lim_{\xi\to\infty} h'(\xi) = 1.$$

The introduction of (24) into (22) gives the component equations

$$\frac{d^2\rho}{d\xi^2} = -\alpha|\boldsymbol{C}_0|\rho\frac{dh}{d\xi}, \qquad \frac{d^2h}{d\xi^2} = \alpha|\boldsymbol{C}_0|\rho\frac{d\rho}{d\xi}. \tag{25}$$

Straightforward integration and use of the boundary conditions gives $\rho = 0$ and $h = \xi$, and hence

$$\hat{\boldsymbol{R}}_0(\xi) = \xi\boldsymbol{N}. \tag{26}$$

We now proceed by solving the $O(\epsilon)$ equation in (19). Use of (26) in (19) and the formation of two successive vector products of the equation with $\boldsymbol{N}$ gives

$$\hat{\boldsymbol{R}}_1''' + \alpha|\boldsymbol{C}_0|\hat{\boldsymbol{R}}_1' = \boldsymbol{C}_1 - \xi\boldsymbol{j} - [\boldsymbol{C}_1\cdot\boldsymbol{N} - \xi\boldsymbol{j}\cdot\boldsymbol{N}]\,\boldsymbol{N}. \tag{27}$$

We can again write

$$\hat{\boldsymbol{R}}_1(\xi) = \rho_1(\xi)\boldsymbol{P} + h_1(\xi)\boldsymbol{N}\,, \tag{28}$$

and substitution of this into (27) gives

$$\rho_1''' + \alpha|\boldsymbol{C}_0|\rho_1' = \boldsymbol{P}\cdot[\boldsymbol{C}_1 - \xi\boldsymbol{j}]\,, \qquad h_1''' + \alpha|\boldsymbol{C}_0|h_1' = 0. \tag{29}$$

Integration of the ρ_1 equation along with the restriction that the shape $\hat{\boldsymbol{R}}(\xi)$ remains a bounded function of s within the boundary layer (which means that ρ_1 can only grow as fast as ξ^2) yields leads to

$$\rho_1 = Be^{-\xi\sqrt{|\boldsymbol{C}_0|}} + \frac{(\boldsymbol{P}\cdot\boldsymbol{j})\xi^2}{2|\boldsymbol{C}_0|} - \frac{(\boldsymbol{P}\cdot\boldsymbol{C}_1)\xi}{|\boldsymbol{C}_0|} + \frac{\boldsymbol{P}\cdot\boldsymbol{j}}{|\boldsymbol{C}_0|^2}. \tag{30}$$

After application of the boundary conditions $\rho_1(0) = h_1(0) = 0$ and $h'(\infty) = 0$, the h_1 equation is found to have only the trivial solution, $h_1 = 0$, so that the complete inner solution up to $O(\epsilon^2)$ has the form:

$$\epsilon\hat{\boldsymbol{R}}(\xi) = \epsilon\xi\boldsymbol{N} + \epsilon^2\left[\frac{\xi^2}{2}\frac{(\boldsymbol{P}\cdot\boldsymbol{j})}{|\boldsymbol{C}_0|} + \xi\frac{(\boldsymbol{P}\cdot\boldsymbol{C}_1)}{|\boldsymbol{C}_0|} + \frac{(\boldsymbol{P}\cdot\boldsymbol{j})}{|\boldsymbol{C}_0|^2}\left(1 - e^{-\xi\sqrt{|\boldsymbol{C}_0|}}\right)\right]\boldsymbol{P} + \ldots. \tag{31}$$

3.3 Matching the Inner and Outer Solutions

The matching between the inner and outer solutions is conducted with the method of intermediate co-ordinates (Kevorkian & Cole 1996). The arclength s and the boundary layer co-ordinate ξ are both expressed in terms of an intermediate co-ordinate $\eta(\epsilon)$ according to

$$s = \eta\tau, \qquad \xi = \frac{\eta\tau}{\epsilon},$$

where $\eta(\epsilon)$ is such that $\eta(\epsilon)$ and $\epsilon/\eta(\epsilon)$ are both $o(1)$, and τ is fixed. Then the inner solution at $s = 0$ has the form:

$$\boldsymbol{R}(s) = \epsilon\hat{\boldsymbol{R}}_0\left(\frac{\eta\tau}{\epsilon}\right) + \epsilon^2\hat{\boldsymbol{R}}_1\left(\frac{\eta\tau}{\epsilon}\right) + \ldots, \tag{32}$$

while the outer expansion becomes

$$\boldsymbol{R}(s) = \boldsymbol{R}_0(\eta\tau) + \epsilon\boldsymbol{R}_1(\eta\tau) + \ldots. \tag{33}$$

The matching process between the inner and outer solutions near $s = 0$ is written as

$$\lim_{\epsilon\to 0}\left\{\epsilon\hat{\boldsymbol{R}}_0\left(\frac{\eta\tau}{\epsilon}\right) + \epsilon^2\hat{\boldsymbol{R}}_1\left(\frac{\eta\tau}{\epsilon}\right) + \ldots\right\} = \lim_{\epsilon\to 0}\{\boldsymbol{R}_0(\eta\tau) + \epsilon\boldsymbol{R}_1(\eta\tau) + \ldots\} \tag{34}$$

and leads to the $O(1)$ and $O(\epsilon)$ conditions:

$$\boldsymbol{0} = \boldsymbol{R}_0(0), \qquad \boldsymbol{0} = \boldsymbol{R}_1(0). \tag{35}$$

A similar matching process between the inner and outer solutions near $s = 1$ yields:

$$d\boldsymbol{i} = \boldsymbol{R}_0(1), \qquad \boldsymbol{0} = \boldsymbol{R}_1(1). \tag{36}$$

Equation $(35)_1$ determines (X_0, Y_0, Z_0) while $(36)_1$ provides a set of three nonlinear equations for the determination of $\boldsymbol{C}_0$. There are two solutions: a tensile solution with $c_x < 0$ and a compressive solution with $c_x > 0$. Since typically the $c_x < 0$ solution is the physically realised one, only this solution is considered in the present study. Equations $(35)_2$ and $(36)_2$ then provide six linear equations for the components of $\boldsymbol{C}_1$ and the integration constants (X_1, Y_1, Z_1), which are all found to be zero. We therefore have that the $O(\epsilon)$ outer solution $\boldsymbol{R}_1 \equiv \boldsymbol{0}$.

Fig. 2 shows a comparison of the analytical results with 'exact' results obtained by numerically integrating the full equation (9). The solid line shows the results of the numerical calculations, while the long dash line shows the two-term outer solution, and the dotted line shows the two-term inner solution. In order to bring out the

boundary layer more clearly, the derivatives of the various solutions rather than the solutions themselves are displayed. The agreement is found to be reasonable for $\epsilon = 0.05$ (Fig. 2a) and to become better for more realistic values of ϵ such as $\epsilon = 0.01$ (Fig. 2b).

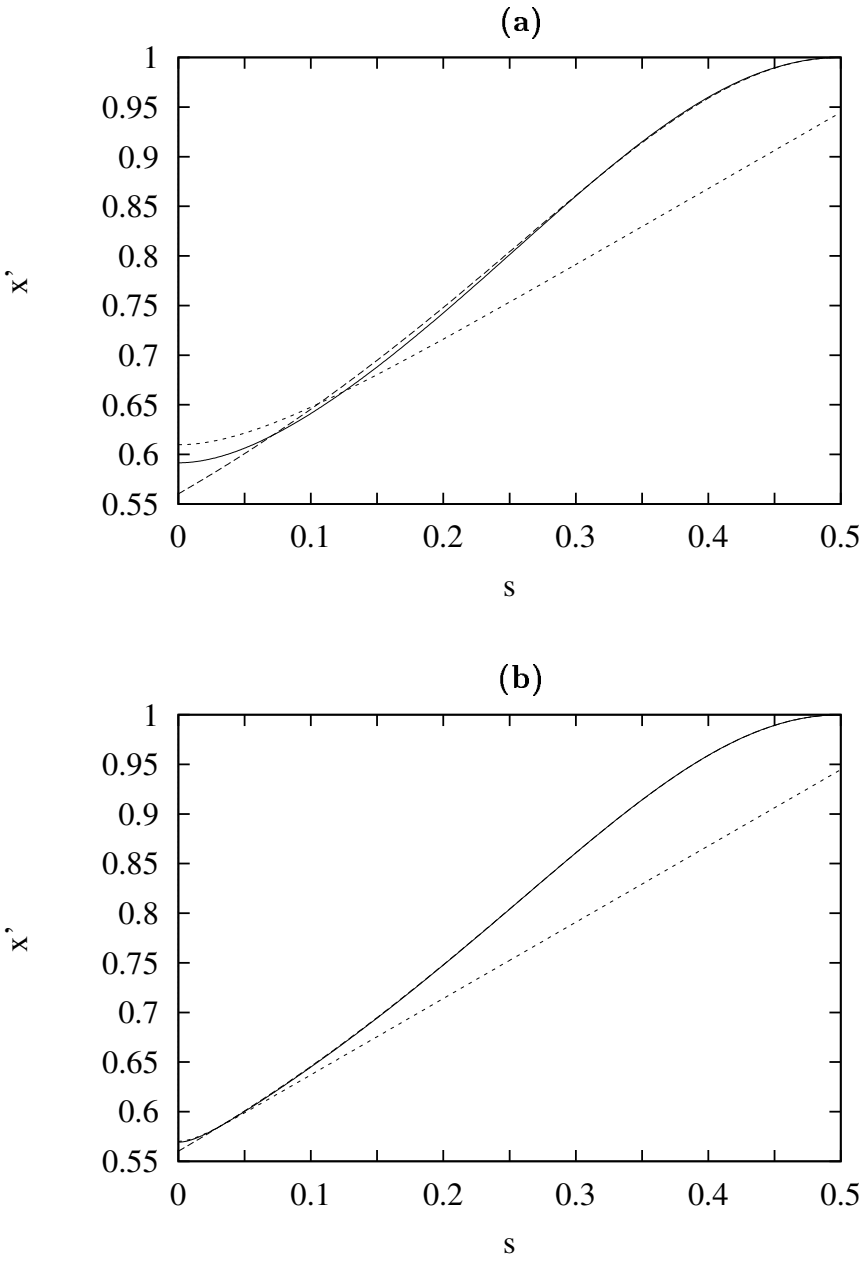

Figure 2: Derivatives of the x components of the outer (dashed), inner (dotted) and exact (solid) solution against arclength s for (a) $\epsilon = 0.05$ and (b) $\epsilon = 0.01$. Half the solutions are displayed. ($d = 0.8,\ \kappa = 3/4$.)

4 High-twist Analysis

In order to solve equation (9) it is useful to introduce an angular description of the tangent vector to the rod which automatically satisfies the inextensibility constraint. A convenient choice in order to avoid polar singularities for the present configuration is to choose Euler angles θ and ϕ which are defined in terms of Cartesian co-ordinates (x, y, z) via

$$\begin{aligned} \boldsymbol{R} &= x\,\boldsymbol{i} + y\,\boldsymbol{j} + z\,\boldsymbol{k}, \\ \boldsymbol{R}' &= \cos\theta\cos\phi\,\boldsymbol{i} + \cos\theta\sin\phi\,\boldsymbol{j} + \sin\theta\,\boldsymbol{k}. \end{aligned} \tag{37}$$

The variable ϕ represents the angle the tangent makes with the horizontal plane, while $\sin\theta$ measures the tangential component in the z-direction.

The expansion of the vector $\boldsymbol{C}$ in terms of Cartesian components,

$$\boldsymbol{C} = C_x\,\boldsymbol{i} + C_y\,\boldsymbol{j} + C_z\,\boldsymbol{k},$$

allows (9) to be expressed as a system of seven first-order differential equations for $(x, y, z, \phi, \theta, \phi', \theta')$. These are given by

$$\begin{aligned} \phi'' &= 2\phi'\,\theta'\tan\theta - \frac{2\pi\kappa T w\,\theta'}{\cos\theta} - \frac{C_x\sin\phi - (C_y - s)\cos\phi}{\varepsilon^2\cos\theta}, \\ \theta'' &= \theta'^2\tan\theta + \left[\frac{F(s)}{\varepsilon^2} - G(s)\right]\tan\theta + 2\pi\kappa T w\,\phi'\cos\theta + \frac{C_z}{\varepsilon^2\cos\theta}, \end{aligned} \tag{38}$$

where the functions $F(s)$ and $G(s)$ are defined by

$$\begin{aligned} F(s) &= s\cos\theta\sin\phi - (C_x\cos\theta\cos\phi + C_y\cos\theta\sin\phi + C_z\sin\theta), \\ G(s) &= \theta'^2 + \phi'^2\cos^2\theta, \end{aligned} \tag{39}$$

together with the definitions of (37):

$$\begin{aligned} x' &= \cos\theta\cos\phi, \\ y' &= \cos\theta\sin\phi, \\ z' &= \sin\theta. \end{aligned} \tag{40}$$

The boundary conditions (10) can be expressed in terms of the seven dependent variables in the obvious way, leading to ten conditions, five at the left end and five at the right. Given that there are also three unknown constants constants (C_x, C_y, C_z), this provides a formally well-posed boundary-value problem that can be solved, for example, using a shooting method.

A further reduction is possible due to the assumed symmetry of the shape about $s = 1/2$. The equations (38)–(40) are invariant under the reversing symmetry

$$\begin{aligned} &x(s) = d - x(1-s), \quad y(s) = y(1-s), \quad z(s) = -z(1-s), \\ &\phi(s) = -\phi(1-s), \quad \theta(s) = \theta(1-s), \quad s \in [0,1]\,, \end{aligned} \tag{41}$$

and from (38) this implies

$$C_y = \frac{1}{2}. \tag{42}$$

For rod shapes which obey (41), one can pose a simpler boundary-value problem with s running over $[0, 1/2]$ by taking

$$\begin{aligned} &x(0) = y(0) = z(0) = 0, \\ &x(1/2) = d/2, \quad z(1/2) = 0, \quad \phi(1/2) = 0, \quad \theta'(1/2) = 0. \end{aligned} \tag{43}$$

The use of (43) in place of (10) results in one less boundary condition and one less scalar unknown since C_y is now fixed by the symmetry. Hence the problem remains formally well-posed, but now has the computational advantages of having to be solved on a smaller domain and being satisfied by a smaller class of solutions within a potential multiplicity.

4.1 Numerical Results

The system of equations (38) and (40), subject to the boundary conditions (43), has been solved using the software package AUTO (Doedel, Champneys, Fairgrieve, Kuznetsov, Sandstede & Wang 1997) for specified values of d, ε, κ, and Tw. This software uses a collocation method which automatically refines grids to capture regions where the solution changes rapidly, such as the boundary layers at the ends of the rod.

The purpose of this section is to study what happens to the catenary-like solution as Tw is increased. All results are presented for a fixed value $\epsilon = 0.01$. Fig. 3 shows a series of profiles computed under increasing Tw for the span lengths $d = 0.99$, 0.95, and 0.80. In each case, the shape remains essentially in the low-twist configuration until a critical twist is reached, at which point the sag begins to decrease as a superimposed helix develops onto the sagged span. As Tw continues to increase, the number of helical turns in the outer region increases and to preserve total arclength, the span centre rises up and the helical radius becomes smaller. Fig. 4 shows plots of the associated end tension $T(0)$ and the magnitude of the centre sag $|y(1/2)|$ versus the applied twist Tw for the three values $d = 0.99$, 0.95, and 0.80.

From Figs 3 and 4 it is clear that the low-twist configuration remains essentially unperturbed until a critical value of Tw is reached. Since there is a gravitational force, the tension in the rod is not constant, so that the Greenhill buckling analysis

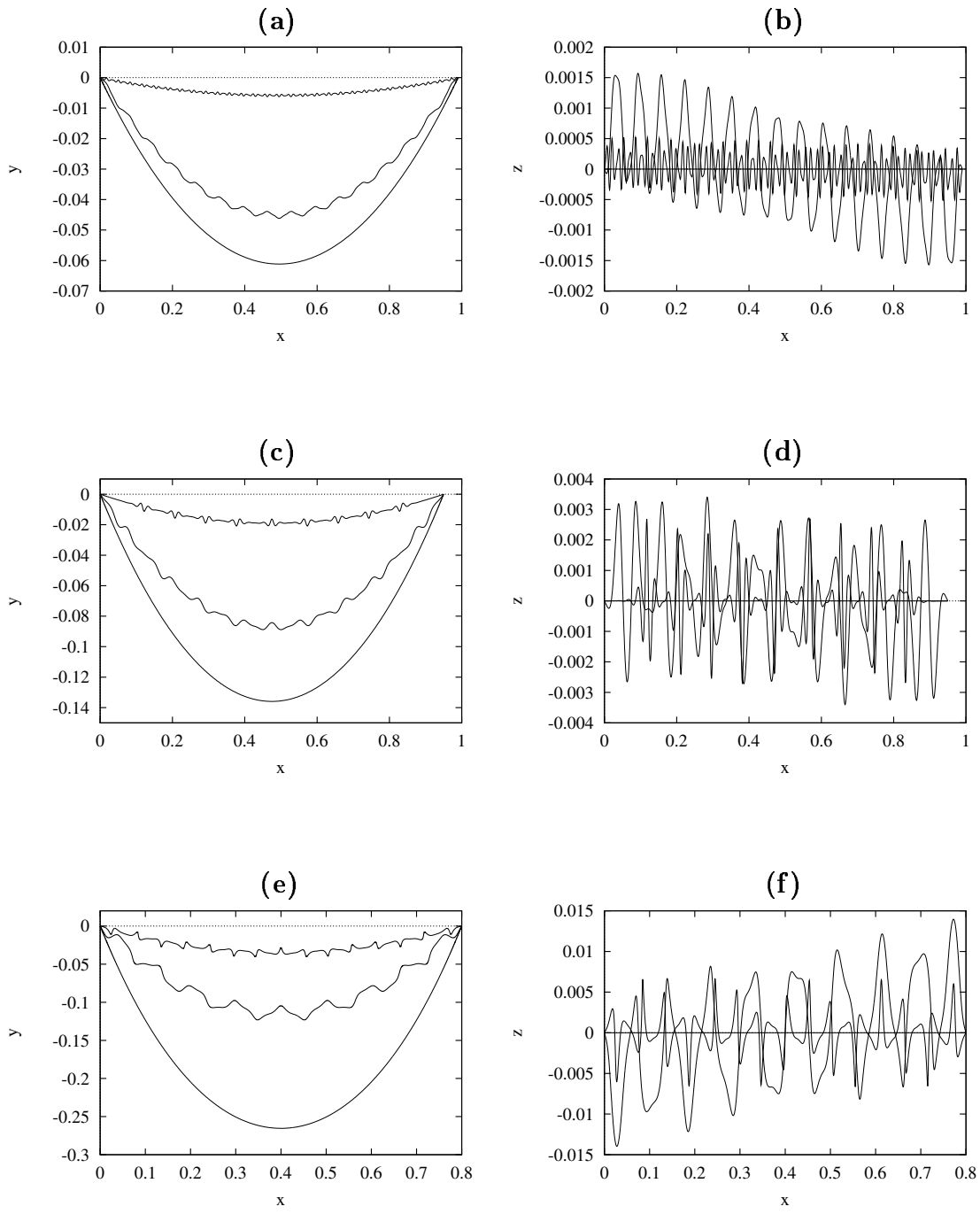

Figure 3: xy and xz projections of the hanging rod at $d = 0.99$ (top), 0.95 (middle) and 0.80 (bottom) ($\epsilon = 0.01,\ \kappa = 3/4$). In (a) and (b), $Tw = 0, 80, 100$; in (c) and (d), $Tw = 0, 50, 100$; in (e) and (f), $Tw = 0, 40, 60$.

does not apply. However, the nondimensional form of the Greenhill buckling formula for a finite-length rod has the form

$$4\pi^2\varepsilon^4 = Q^2 - 4\varepsilon^2 T(0),$$

where the end tension $T(0)$ has been used. The torque Q is eliminated in terms of the twist Tw with $(9)_6$ and the resulting estimate for the critical twist Tw_c for Greenhill-like buckling is

$$Tw_c = \sqrt{\frac{1}{\kappa^2} + \frac{T(0)}{\kappa^2\pi^2\varepsilon^2}} \sim \frac{\sqrt{T(0)}}{\kappa\pi\varepsilon}.$$

The estimates of the critical twist Tw_c for the span lengths $d = 0.99$, 0.95, and 0.80 based on the tension $T(0)$ associated with the zero-twist solution (ie. $Tw = 0$) are respectively 61, 42, 33. These compare to the values 61, 42, and 35 at the sharp transition points in Fig. 4. At the transition points in Fig. 4, the nature of the solution in the outer region begins to change. This can be seen in the associated rod shapes of Fig. 3. The post-transition solution consists of a catenary-like solution across the span with a superimposed helix-like solution which has a period of $O(\varepsilon)$.

As Tw continues to increase, the number of helical turns increases so that the sag and helical amplitude both decrease to preserve total arclength.

Notice that the helix-like solution superimposed on the catenary in general appears to be quasi-periodic. Moreover, after an initial jump at the transition point the amplitude of the helix decreases with Tw. These effects can be seen more clearly in Fig. 5 which shows in details a computation for $d = 0.98$. In fact, after the initial jump the helix amplitude (which can be estimated by taking the average of the oscillations in Fig. 5(b)) appears to behave roughly as the square root of the sag $|y(d/2)|$ depicted in (a). Also note that the oscillations in the maximum of $z(s)$ indicate that the solution is a modulated helix with the maximum amplitude of the modulation rotating in the (y, z)-plane as Tw is increased. This is further emphasised by panels (c) and (e) of Fig. 5 which show solutions that are approximately quasi-periodic. However, at certain isolated values of Tw, the frequency of the helix and its modulation may hit resonance resulting a solution that is approximately periodic as indicated in (d) and (f).

For lower values of d (e.g. $d = 0.95$ and $d = 0.8$ illustrated in Fig. 3(b),(c)) it is apparent that as Tw is further increased the helix-like response develops a localised profile. That is, it develops the characteristics of a chain of wavepackets. For Tw-values higher than those depicted, it became problematical numerically to continue

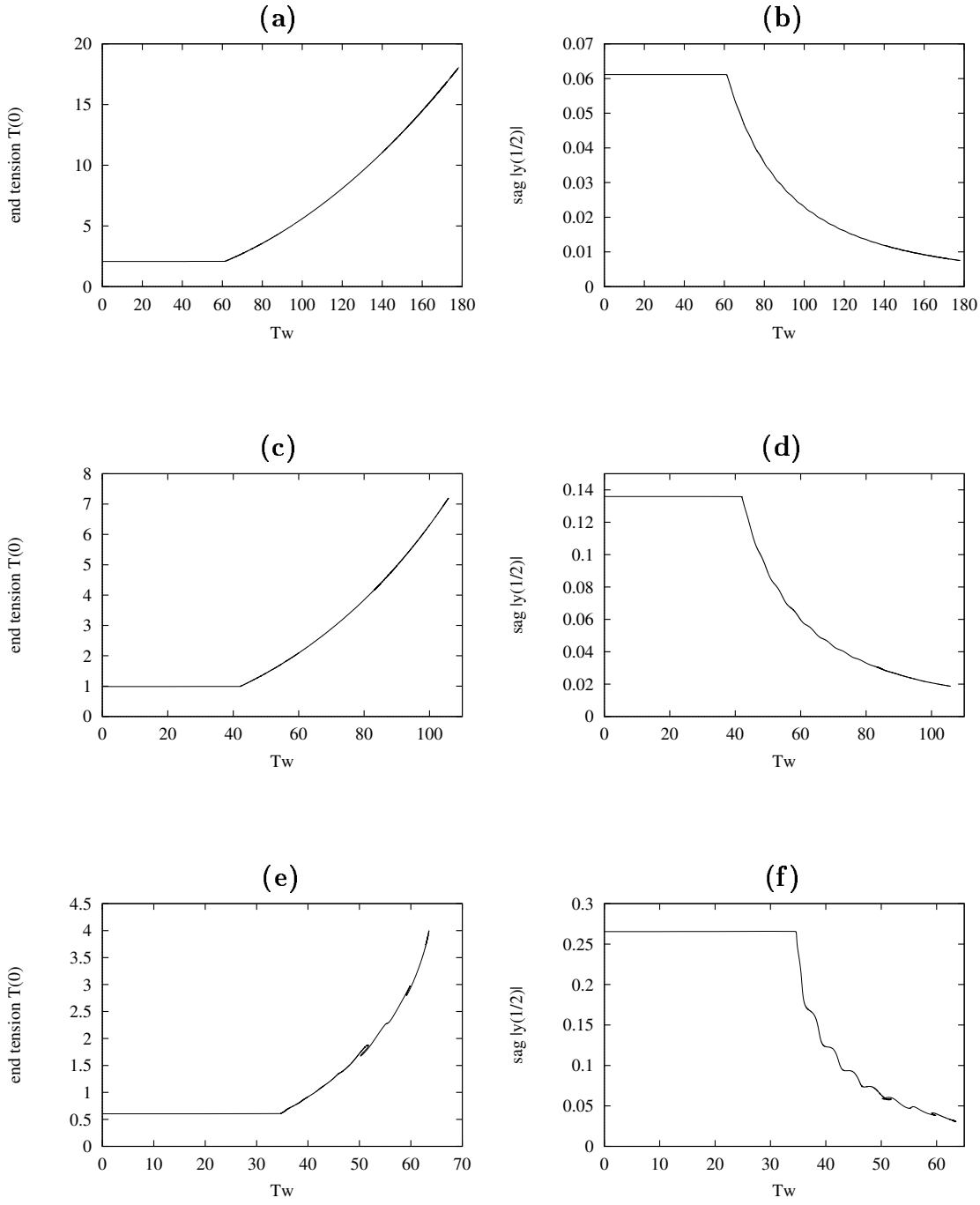

Figure 4: End tension $T(0)$ and sag $|y(1/2)|$ against total twist Tw at $d = 0.99$ (top), 0.95 (middle) and 0.80 (bottom) ($\epsilon = 0.01,\ \kappa = 3/4$).

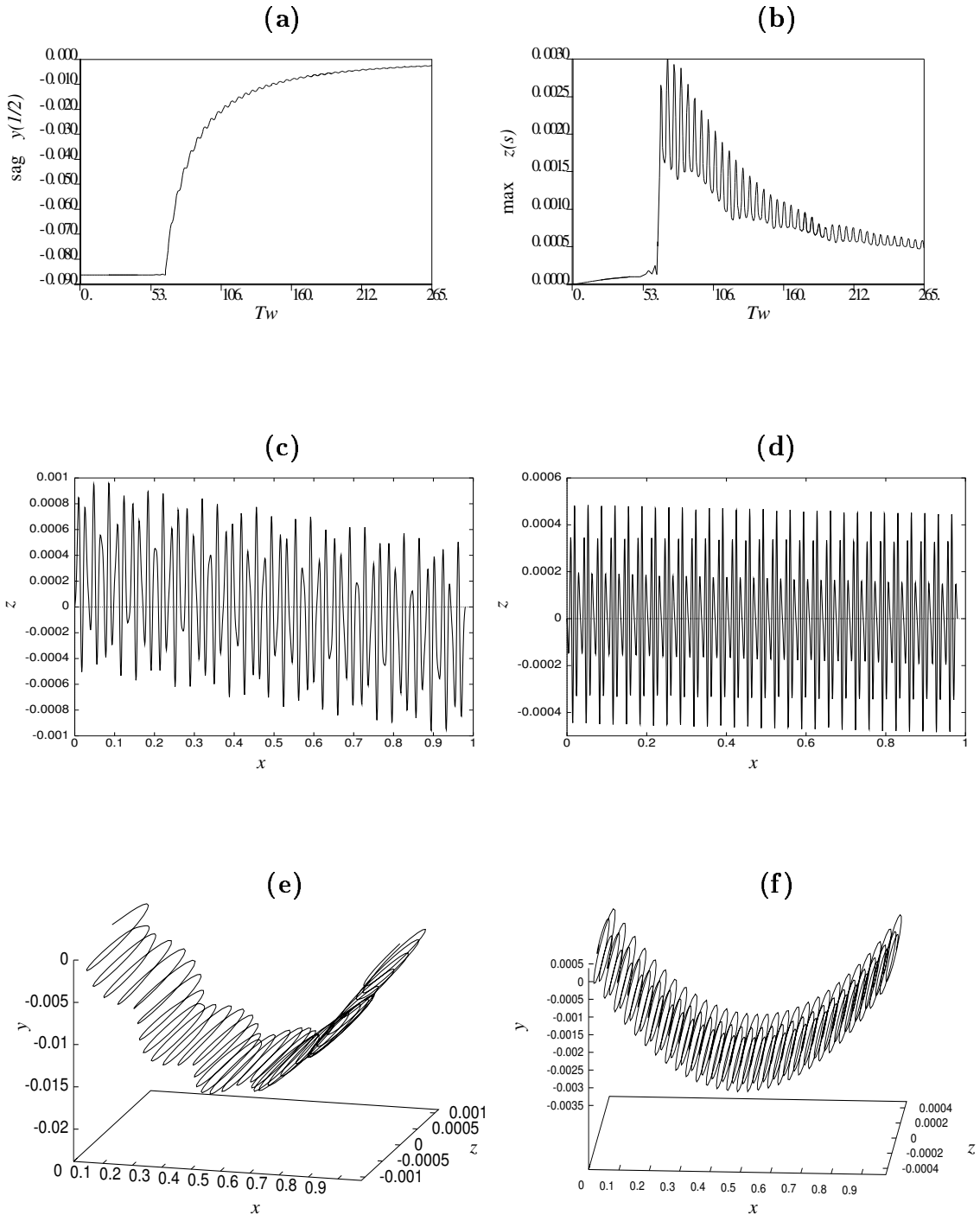

Figure 5: Further details of a computation for $d = 0.98$ ($\varepsilon = 0.01$, $\kappa = 3/4$). **(c)** and **(d)** show projections of solutions at $Tw = 170$ and 265 respectively and **(e)** and **(f)** show 3D rod shapes at $Tw = 212$ and 265 respectively.

the branch of solutions but there was evidence to suggest that the localization process continues until presumably the rod starts to self-intersect and writhe into a double helix. Some of the causes of these numerical difficulties shall be commented on the Discussion section which follows the multi-scale analysis below.

Instead, Fig. 6 presents results for the lower value of $\varepsilon = 0.1$ where it is possible to compute to the limit of large Tw more reliably. Note from panels (c) and (d) the behaviour for $d = 0.98$. Compared with the results for $\varepsilon = 0.01$, there is less distinction between the low-twist and high-twist regimes and the sharp transition at $Tw = Tw_c$ has been smoothed out, as should be expected because ε is now of moderate size. As Tw is increased, only a small number of helical waves are fitted in, before a marked localisation takes place towards the centre of the rod. At $Tw = Tw_j \approx 40.7$ the localisation is so extreme that the sag of the catenary has almost disappeared and, precisely at the mid-point of the rod, the tangent vector lies in the z-direction. It is problematical to compute the branch for any higher Tw-values because the polar representation (37) now breaks down. However, given that the loading is approximately in the (x, y)-plane, then the condition of Coyne (1990) states that at such a point where the tangent points directly out of the plane the rod would dynamically jump into a self-intersecting solution. Upon further increase of Tw writhing into a double helical ply plus an end loop (as described in Stump, Fraser & Gates (1998)) would presumably occur. Fig. 6(b) shows how Tw_j varies with d for $\varepsilon = 0.1$. Note that a degree of sensitivity to d was found in determining whether the localisation 'writhes down' (with $y(1/2) < 0$) as in Fig. 6(c)) or 'writhes up' (with $y(1/2) > 0$).

4.2 Multi-scaling Analysis

The numerical results for the shallow hanging rod show that a sudden transition in behaviour occurs for Tw of $O(1/\varepsilon)$. The governing equation (9) continues to apply, but the separation of length scales between the inner and outer layers which occurs for $Tw \sim O(1)$ does not hold for $Tw \sim O(1/\varepsilon)$. Instead, the numerical results suggest that the outer solution develops a multiple-scale character consisting of: a catenary-like portion on the scale s; and a superimposed helical solution with a wavelength of $O(\epsilon)$. This suggests a multi-scaling analysis in which $\boldsymbol{R}'(s)$ is replaced with $\boldsymbol{F}(s, \xi)$ and derivatives with respect to s are replaced by:

$$\frac{d}{ds} = \frac{\partial}{\partial s} + \frac{1}{\varepsilon}\frac{\partial}{\partial \xi}\,.$$

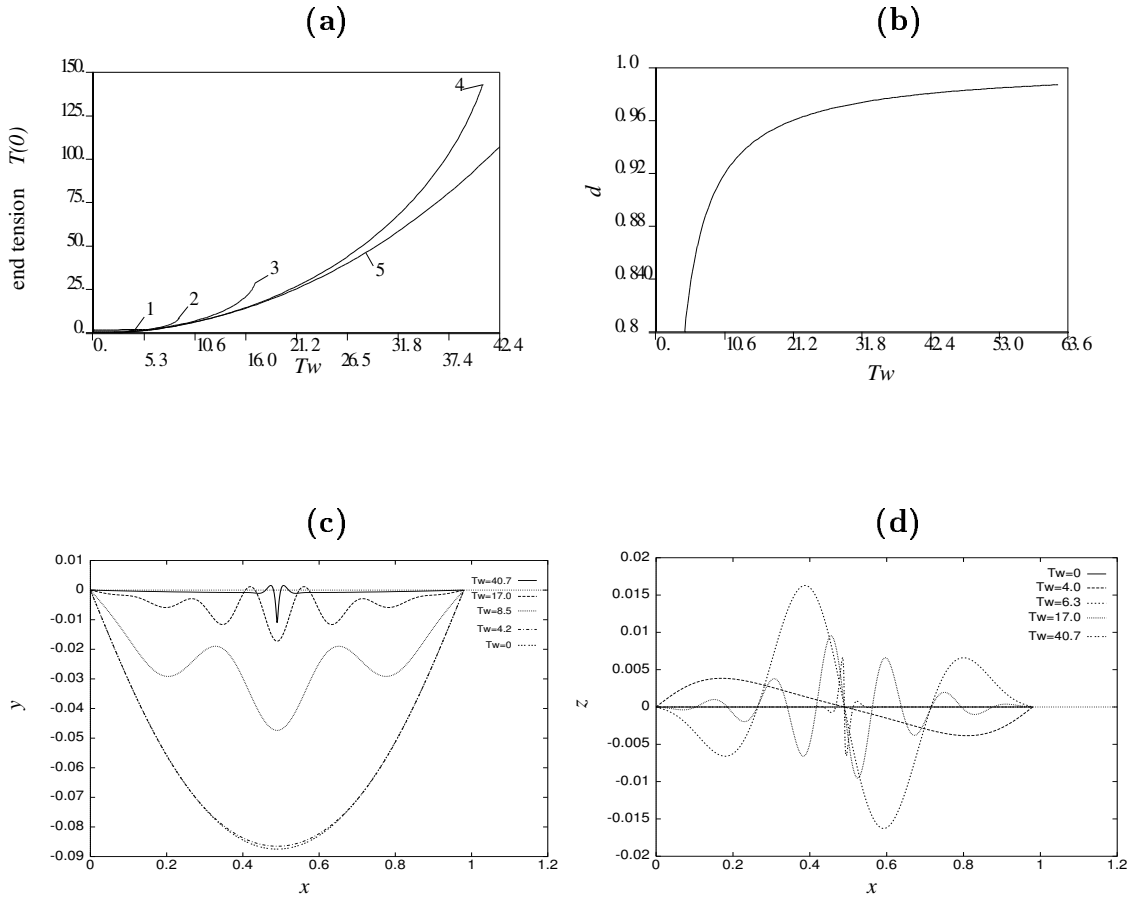

Figure 6: Results for $\varepsilon = 0.1$ ($\kappa = 3/4$). **(a)** End tension $T(0)$ against total twist Tw for: (1) $d = 0.8$; (2) $d = 0.9$; (3) $d = 0.95$; (4) $d = 0.98$; (5) $d = 0.99$. Branches (1)-(4) end at 'jump points' where the rod points entirely in the z-direction; branch (5) can be continued beyond the scale depicted. **(b)** Locus of jump points in the (Tw, d)-plane. **(c),(d)** xy and xz projections along the curve for $d = 0.98$ at the annotated Tw-values.

With the definition of the $O(1)$ variable

$$q = 2\pi\kappa\epsilon T w,$$

the governing equation (9) becomes

$$\begin{aligned} &q\varepsilon \boldsymbol{F}\times\boldsymbol{F}_s + q\boldsymbol{F}\times\boldsymbol{F}_\xi - \varepsilon^2\boldsymbol{F}_{ss} - 2\varepsilon\boldsymbol{F}_{s\xi} - \boldsymbol{F}_{\xi\xi} - \\ &-\varepsilon^2\boldsymbol{F}(\boldsymbol{F}_s\cdot\boldsymbol{F}_s) - 2\varepsilon\boldsymbol{F}(\boldsymbol{F}_s\cdot\boldsymbol{F}_\xi) - \boldsymbol{F}(\boldsymbol{F}_\xi\cdot\boldsymbol{F}_\xi) + \\ &\boldsymbol{F}[s(\boldsymbol{F}\cdot\boldsymbol{j}) - \boldsymbol{F}\cdot\boldsymbol{C}] - s\boldsymbol{j} + \boldsymbol{C} = \boldsymbol{0}, \end{aligned} \tag{44}$$

where the subscripts denote differentiation with respect to that variable. This equation is sufficiently complicated that we confine our interest to the nature of the outer solution to leading order and attempt only to separate the leading-order behaviour on the different scales.

Let us formally suppose that

$$\boldsymbol{F} = \boldsymbol{H}(s) + \boldsymbol{G}(\xi) \tag{45}$$

where for the sake of book-keeping both $\boldsymbol{H}$ and $\boldsymbol{G}$ are assumed to be $O(1)$ (although we shall see later that this assumption is not necessary). Then to leading order (44) becomes

$$\begin{aligned} O(1): \qquad & q(\boldsymbol{H}+\boldsymbol{G})\times\dot{\boldsymbol{G}} - \ddot{\boldsymbol{G}} - (\boldsymbol{H}+\boldsymbol{G})(\dot{\boldsymbol{G}}\cdot\dot{\boldsymbol{G}}) + \\ & (\boldsymbol{H}+\boldsymbol{G})[s(\boldsymbol{H}+\boldsymbol{G})\cdot\boldsymbol{j} - (\boldsymbol{H}+\boldsymbol{G})\cdot\boldsymbol{C}] - s\boldsymbol{j} + \boldsymbol{C} = 0, \end{aligned} \tag{46}$$

where an over dot denotes differentiation with respect to ξ.

Now, if we treat s and ξ as independent co-ordinates, (46) must be interpreted differently on the two different length scales. On the *long* scale $\boldsymbol{G}$ and its derivatives may be replaced by their averages over the shorter length scale. Based on the numerical evidence, we seek solutions for $\boldsymbol{G}$ that are periodic or quasiperiodic perturbations about some fixed vector. Hence we take

$$\langle\boldsymbol{G}\rangle = \boldsymbol{D}, \quad \langle\dot{\boldsymbol{G}}\rangle = \boldsymbol{0}, \quad \langle\ddot{\boldsymbol{G}}\rangle = \boldsymbol{0}\,,$$

where: $\langle\cdot\rangle$ represents the average value, and $\boldsymbol{D}$ is an unknown constant vector. Upon setting $\tilde{\boldsymbol{H}} = \boldsymbol{H} + \boldsymbol{D}$, (46) then becomes

$$\tilde{\boldsymbol{H}}[s(\tilde{\boldsymbol{H}}\cdot\boldsymbol{j}) - \tilde{\boldsymbol{H}}\cdot\boldsymbol{C}] - s\boldsymbol{j} + \boldsymbol{C} = 0\,. \tag{47}$$

This equation up to boundary conditions and constant of integration $\boldsymbol{C}$ is precisely equivalent to the $O(1)$ part of equation (12) whose solution (13) describes the outer

catenary of the untwisted rod. Since we are interested in almost flat solutions, for which the span d is close to one, we expand the constant

$$\boldsymbol{C} = -\tilde{T}\,\boldsymbol{i} + C_y\,\boldsymbol{j} + \text{h.o.t.}$$

where: C_y is $O(1)$; and $\tilde{T}$ is the as yet unknown constant rod tension.

In contrast, on the *short* length scale we look at some specific arclength s_0 ($0 < s_0 < 1$) along the rod and replace s by $s_0 + \varepsilon\xi$. Then to leading order (46) becomes

$$O(1): \quad q\tilde{\boldsymbol{G}} \times \dot{\tilde{\boldsymbol{G}}} - \ddot{\tilde{\boldsymbol{G}}} - \tilde{\boldsymbol{G}}(\dot{\tilde{\boldsymbol{G}}} \cdot \dot{\tilde{\boldsymbol{G}}}) - \tilde{\boldsymbol{G}}[\tilde{\boldsymbol{G}} \cdot \tilde{\boldsymbol{C}}] + \tilde{\boldsymbol{C}} = 0, \tag{48}$$

where $\tilde{\boldsymbol{C}} = \boldsymbol{C} - s_0\boldsymbol{j}$ and $\tilde{\boldsymbol{G}} = \boldsymbol{G} + \boldsymbol{H}(s_0)$ with $\boldsymbol{H}(s_0)$ regarded as a constant vector. But (48) is nothing other than the derivative of the dimensionless equation for a free rod subject to a terminal force $\tilde{\boldsymbol{C}}$ and twisting moment q, equivalent for example to (Stump et al. 1998, Eq. 4.1). Since this equation is posed over the short length scale, the rod is long ($L = 1/\varepsilon$). The rod is also naturally straight since (48) is autonomous in ξ. Now we assume that the precise effects of the boundary conditions are negligible other than to apply a remote torque q and the unknown remote tension $\tilde{T}$.

Equation (48) possesses a rich variety of postbuckling solutions for $q^2 < 4\tilde{T} + O(\varepsilon^2)$ (cf. (1) where $B = 1$ due to nondimensionalisation). For an up to date account of all such solutions, including helices, modulated helices and localised helices, see van der Heijden & Thompson (1999). The simplest non-trivial solution is the helix which is given by

$$\tilde{\boldsymbol{G}} = \cos\beta\boldsymbol{e}_1 + \cos\psi(\xi)\sin\beta\boldsymbol{e}_2 + \sin\psi(\xi)\sin\beta\boldsymbol{e}_3,$$

where $\boldsymbol{e}_1$ is along the direction of the loading axis and $\boldsymbol{e_2}$ and $\boldsymbol{e}_3$ are chosen so as to form an orthonormal basis, and the angular description of the helix satisfies

$$\psi = \sqrt{\tilde{T}}\,\xi, \quad 1 + \cos\beta = q/\sqrt{\tilde{T}}.$$

From these expressions we can calculate the end-shortening $\mathcal{E}$ associated with the helix

$$\mathcal{E} = (1 - \cos\beta)L = (2 - q/\sqrt{\tilde{T}})/\varepsilon, \tag{49}$$

and the amplitude a of the helix given by

$$a = (1/q)\sin\beta(1 + \cos\beta) = \frac{q}{\tilde{T}}\sqrt{2\frac{\sqrt{\tilde{T}}}{q} - 1} \tag{50}$$

We now return to the long scale equation (47) and, remembering that we have taken $1-d$ as small, we write the solution

$$\tilde{H} = \frac{\tilde{T}}{\sqrt{\tilde{T}^2 + \left(s - \frac{1-\mathcal{E}}{2}\right)^2}}\,\boldsymbol{i} + \frac{\left(s - \frac{1-\mathcal{E}}{2}\right)}{\sqrt{\tilde{T}^2 + \left(s - \frac{1-\mathcal{E}}{2}\right)^2}}\,\boldsymbol{j} + \text{h.o.t.}$$

where we have evaluated the end condition at $s = 1-\mathcal{E}$ rather than at 1. The physical shape is obtained by evaluating $\boldsymbol{R} = \int \boldsymbol{H}(s)$, which leads to the end condition

$$d = 2\tilde{T}\sinh^{-1}\left(\frac{1-\mathcal{E}}{2\tilde{T}}\right), \tag{51}$$

and the sag $|y((1-\mathcal{E})/2)|$ given by

$$\text{sag} = \sqrt{\tilde{T}^2 + \frac{(1-\mathcal{E})^2}{4}} - \tilde{T}.$$

Now (51), given (49), is a nonlinear equation for determining $\tilde{T}$ in terms of ε, q and d. In the limit of large $\tilde{T}$, the solution to this equation can be approximated by

$$\tilde{T} = \frac{q^2}{2} + \text{h.o.t.} = \pi^2\kappa^2\varepsilon^2 T w^2 + \text{h.o.t.}$$

Back substitution then gives

$$\mathcal{E} = 1 - d + \text{h.o.t.},$$

$$a = \frac{\sqrt{8\varepsilon(1-d)}}{q} + \text{h.o.t.} = \frac{\sqrt{2(1-d)}}{\sqrt{\varepsilon}\pi\kappa T w} + \text{h.o.t}$$

and

$$\text{sag} = \frac{1}{4}(\sqrt{q^4 + 4d^2} - q^2) = \frac{d^2}{8\pi^2\kappa^2\varepsilon^2 T w^2} + \text{h.o.t}$$

In all of these expressions, h.o.t. refers to terms which are smaller as $1-d \to 0$, $\varepsilon \to 0$ and $q \to \infty$.

These results agree with the qualitative scalings that may be deduced from the numerics. In particular as Tw is increased well beyond Tw_c, the end tension $T(0) = \tilde{T}$ scales like q^2 i.e. $\tilde{T} \propto \varepsilon^2 T w^2$, and the sag scales like the square of the amplitude of the helix with both tending to zero as $Tw \to \infty$.

Finally let us comment on the original assumption that both $\boldsymbol{H}(s)$ and $\boldsymbol{G}(\xi)$ were $O(1)$. As we have now seen we never actually solve equations for these quantities, but instead deal with the modified quantites $\tilde{\boldsymbol{H}}$ and $\tilde{\boldsymbol{G}}$, both of which are indeed $O(1)$ and are coupled through the contants $\boldsymbol{D}$ and $\tilde{\boldsymbol{C}}$. In fact there is some indeterminacy in what part of the solution for $\boldsymbol{F}$ in the $\boldsymbol{i}$ direction is regarded as belonging to $\boldsymbol{H}$ and what part belonging to $\boldsymbol{G}$.

5 Discussion

In this paper we have demonstrated, via close agreement between numerics and asymptotics, two distinct regimes of a rod hanging under gravity subject to an applied twist. For rods of fixed material properties the dimensionless parameter ε may be regarded as the aspect ratio of the rod, with $\varepsilon \to 0$ being the limit of a long thin rod. For twist of order much less than this aspect ratio, the effect of applying torsion to a hanging catenary is negligible except in boundary layers of proportion $O(1/\varepsilon)$ of the rod's length. The present study has considered simply supported ends, in which case the boundary layer leads to sharp transitions only in the rate of change of the rod curvature. This contrasts with the situation for clamped boundary conditions where the analysis of Stump & van der Heijden (1998) (which albeit had a different overall geometry) shows that the sharp transitions occur in the rod tangent.

We have then seen that at approximately the classical Greenhill buckling twist (suitably rescaled) $Tw = Tw_c \approx \sqrt{T}/(\pi\kappa\varepsilon)$, the response changes markedly over a short range of Tw to a catenary with a super-imposed helical deformation. The process of this transition we have not described in detail, but is akin to an imperfect bifurcation, with either ε or $1 - d$ playing the role of the imperfection parameter.

The second regime holds sway for $Tw > Tw_c$ and we have been able to motivate what was observed in careful numerical experiments via a heuristic double-scale analysis. This reveals that by looking on the appropriate length scales one recovers either the equation for a free rod subject to tension and torsion or that for a torsion free rod hanging under gravity. The former is known to be completely integrable and admit solutions in the form of helices and modulated helices. The latter has the well-known catenary solution. These solutions were then matched by assuming that the helix supplies an effective end shortening to the arclength of the catenary. This then enabled us to uncover the numerically suggested scalings for the end tension, the sag of the catenary and the amplitude of the superimposed catenary as $Tw \to \infty$.

However, the numerics reveal that one cannot pass to the limit $Tw \to \infty$ and in fact there is a third regime where the helical response (which is in general a modulated periodic waves) localises to the extent that it self intersects. Presumably for higher Tw, the rod will go on to writhe into double helical plies joined by end loops as is known to occur for the gravity-free problem, although such solutions are beyond the scope of the present analysis. The evidence from Fig. 6 suggests that this writhing

regime begins for $Tw = O(1/(\varepsilon(1-d))$.

Another limitation of the double-scale asymptotics is that they do not capture the precise features of the helical solutions on the small scale. These appear in general as quasi-periodic modulated helices rather than a purely periodic response as assumed in the analysis.

Some comments are in order on the accuracy and repeatability of the numerical results. All presented bifurcation curves were computed using AUTO with error tolerances $O(10^{-6})$ and typically 200 collocation intervals with 4 collocation points in each interval. The differential equations were posed on the half-interval $0 < s < 1/2$ using the symmetry conditions (43). Preliminary numerical experiments over the full interval $0 < s < 1$ revealed qualitatively similar results, but the computations were found to be far less robust. Typically numerical continuation would break down for lower Tw-values (even after doubling the number of collocation intervals in AUTO) and would be characterized by a precursive jump to a symmetry-broken state before non-convergence was encountered.

Even using the half-interval formulation, problems were sometimes encountered with non-repeatability of numerical results in resolving the fine features of solutions for $Tw > Tw_c$. Loops in the post-buckled path as in Fig. 4(e),(f) could sometimes be missed unless stepsize tolerances were chosen small enough. Also, as mentioned at the end of section 4.1, for the five branches displayed in Fig. 6(a), where $\varepsilon = 0.1$, it was sometimes found that the rod writhed up and sometimes writhed down. It would appear that there are multiple possible solution paths in the high-twist regime but that only one of these is the fundamental path which is connected to the boundary layer solution as $Tw \to 0$. For smaller ε, like the solutions displayed in Fig. 3(e),(f), there appear to be many points at which the rod's deflection is localizing, yet in a physical experiment self-intersection and a subsequent jump would occur at only one point along the rod's length. Clearly there is a sensitivity to the boundary conditions, especially to the value of d.

While we have focused only on simply supported boundary conditions, preliminary numerical experiments have been performed in the case of a clamped rod. A similar high-twist region was uncovered, with helices superimposed on an underling catenary but the numerical sensitivity seemed even more problematical, perhaps due to the sharper boundary layers.

One message of the present work is that, contrary to the assumptions of Champneys et al. (1997), it is not reasonable to assume that gravity is a small perturbing parameter except in the case of high initial tension $T(0)$ of the untwisted rod (i.e. d close to 1). For example, contrast the findings of the present study with what would happen in the gravity free problem of a long straight rod under dead loading where applied twist Tw is held constant and the ends shortened while remaining under tension (Thompson & Champneys 1996, Fig. 14). There, the initial postbuckling response would be a localised helix (that is, one for which the modulation has infinite period). As end-shortening were further increased, this localisation quickly would become more severe with the rod jumping into a writhing configuration sooner. In the present analysis, where admittedly Tw is now the control parameter, before such localisation and writhing can take place the rod must take up the sag in the catenary, which requires a large amount of extra applied twist. During this process the buckling response is not a localised helix but a periodically modulated one.

Clearly the present study is only a first step towards a full understanding of the behaviour of twisted rods hanging under gravity. Nevertheless, it is one that concurs qualitatively with phenomenological experiments (Thompson & Champneys 1996, Fig 6). Future work should include; a quantitative comparison with experiments, an exploration of the transition as an imperfect bifurcation, including the possibility of multiple solution branches; proper consideration of other boundary conditions such as clamped; and the effects of other 'perturbing' influences like intrinsic curvature, anisotropy or axial extensibility of the rod.

Acknowledgements

This work was largely carried out during visits by ARC and GvdH to the University of Queensland. The work of ARC has been supported by an Ethel Raybold foundation visiting fellowship and the U.K. EPSRC programme. GvdH has been supported by an Australian Research Council grant.

References

Antman, S. (1995), *Nonlinear problems of elasticity*, Springer-Verlag, Berlin. AMS 107.

Champneys, A., van der Heijden, G. & Thompson, J. (1997), 'Spatially complex localisation after one-twist-per-wave equilibria in twisted circular rods with initial curvature', *Phil. Trans. Roy. Soc. Lond. A* **355**, 2151–2174.

Coyne, J. (1990), 'Analysis of the formation and elimination of loops in twisted cable', *IEEE J. Oceanic Eng.* **15**, 71–83.

Doedel, E., Champneys, A., Fairgrieve, T., Kuznetsov, Y., Sandstede, B. & Wang, X. (1997), 'AUTO97: Continuation and bifurcation software for ordinary differential equations'. Available by anonymous ftp from `ftp.cs.concordia.ca`, directory `pub/doedel/auto`.

Goriely, A. & Tabor, M. (1998), 'Spontaneous helix–hand reversal and tendril perversion in climbing plants', *Phys. Rev. Lett.* **80**, 1564–1567.

Greenhill, A. (1883), 'On the strength of shafting when exposed both to torsion and end thrust', *Inst. Mech. Eng. Proc.* **1883**, 182–209.

Kehrbaum, S. & Maddocks, J. (1997), 'Elastic rods, rigid bodies, quaternions and the last quadrature', *Phil. Trans. Roy. Soc. Lond.* **355**, 2117–2136.

Kevorkian, J. & Cole, J. (1996), *Multiple Scale and Singular Perturbation Methods*, Springer-Verlag, New York.

Kirchhoff, G. (1859), 'Über das Gleichgewicht und die Bewegung eines unendlich dünnen elastischen Stabes', *J. für Mathematik (Crelle)* **56**, 285–313.

Love, A. (1927), *A Treatise on the Mathematical Theory of Elasticity*, 4th ed. edn, Cambridge University Press, Cambridge.

Stump, D. & van der Heijden, G. (1998), 'Analytical formulation of a pipe string from a boat: the 3-dimensional bent and twisted rod under gravity'. Submitted to *J. Eng. Math.*

Stump, D., Fraser, W. & Gates, K. (1998), 'The writhing of circular cross-section rods: undersea cables to DNA supercoils', *Proc. Roy. Soc. Lond. A* **454**, 2123–2156.

Thompson, J. & Champneys, A. (1996), 'From helix to localised writhing in the torsional post-buckling of elastic rods', *Proc. Roy. Soc. Lond. A* **452**, 117–138.

Timoshenko, S. & Gere, J. (1961), *Theory of elastic stability*, McGraw-Hill, New York.

van der Heijden, G. & Thompson, J. (1999), 'Helical and localised buckling in twisted rods: a unified analysis of the symmetric case', *Nonlinear Dynamics*.